Article

Characteristics and Genesis of Pore–Fracture System in Alkaline Lake Shale, Junggar Basin, China

Yifan Jiao [1,2], Xianglu Tang [1,2,*], Wenjun He [3], Liliang Huang [3], Zhenxue Jiang [1,2], Leilei Yang [1,2] and Caihua Lin [1,2]

1 National Key Laboratory of Petroleum Resources and Engineering, China University of Petroleum (Beijing), Beijing 102249, China; j247018642f@163.com (Y.J.)
2 Unconventional Petroleum Research Institute, China University of Petroleum (Beijing), Beijing 102249, China
3 Research Institute of Exploration and Development, Xinjiang Oilfield Company, PetroChina, Karamay 834000, China
* Correspondence: tangxl@cup.edu.cn

Abstract: Unconventional oil and gas resources are indispensable, and shale oil is one of them. The Junggar Basin is a typical superposition oil and gas basin in China, with reserves of 100 million tons in many areas and various types of oil and gas reservoirs. The Permian Fengcheng Formation in Mahu Sag has great potential for oil generation, making the study of the Fengcheng Formation reservoir in Mahu Sag particularly important. Based on previous studies, the core sample from well Maye-1 is divided into four lithologies according to mineral composition: felsic shale, dolomitic felsic shale, clay-bearing felsic shale, and siltstone interlayers. Through core observation and description, it is found that the macroscopic porosity of each lithology is well-developed, with felsic shale exhibiting the highest macroscopic fracture density, followed by siltstone interlayers, and clay-bearing felsic shale showing the least development. Argon ion polishing scanning electron microscopy (SEM) and nuclear magnetic resonance (NMR) techniques show that the siltstone interlayer pore development is the best, with pore sizes ranging from 100 to 4000 nm. The fracture development of dolomitic felsic shale is the most significant, with fractures contributing up to 80.14%. The porosity of clay-bearing felsic shale is only 1.12%. The development of pores and fractures in the study area is related to sedimentary tectonic factors and diagenesis. It mainly exhibits three types of subfacies deposits, namely semi-deep lake subfacies, shallow lake subfacies, and lakeshore lake subfacies, predominantly composed of felsic shale. Strong tectonic movements contribute to the formation of macroscopic fractures. Diagenesis plays a crucial role in the formation of microscopic pores. The Fengcheng Formation is primarily influenced by compaction, pressure dissolution, dissolution, and metasomatism. These various diagenetic processes collectively promote the formation of pores, ultimately leading to the development of a multi-scale porosity system in the Fengcheng Formation.

Keywords: pore development; multi-scale; SEM; NMR; core observation

1. Introduction

Nowadays, with the continuous development of oil and gas resources, unconventional oil and gas resources have become an indispensable part. Pyroclastic oil and gas reservoirs have been discovered in many basins in China [1], and shale oil is an important component of unconventional oil and gas resources, attracting much attention from countries around the world [2,3]. The Junggar Basin is a typical superposition oil-bearing basin in western China. Two major petroliferous areas, Kewu and Mahu, have been successively discovered in the fault zone and the sag slope area, forming multiple 100 million-ton reserves, and various types of oil–gas reservoirs have been discovered [4]. The Permian Fengcheng Formation in Mahu Sag is formed by the interlayer deposition of lacustrine shale and dolomitic rock, holding great potential for oil generation [5]. In the relevant studies of shale

oil reservoirs, the pore structure of reservoir shale is of paramount importance [6]. Shale pores serve not only as storage spaces but also as migration channels. Therefore, relevant studies on shale reservoir pore structure are of significant importance [7,8].

Lithofacies refers to the types of rocks and their combinations formed in certain sedimentary environments [9–11]. In different regions, due to variations in sedimentary environments and processes, there are often different divisions of lithofacies. Influenced by differences in material composition and diagenetic states, shale reservoirs of different lithofacies exhibit varying mineral compositions, organic matter contents, and pore structure distributions [11].

The research methods of reservoir pore structure are generally divided into two methods: direct observation and indirect tests. Direct observation is to observe and describe the samples directly by means of core description and observations using optical microscopy and scanning electron microscopy. The indirect test indirectly obtains the distribution of the pore structure inside the sample by calculating by filling the sample with fluid or gas, including high-pressure mercury injection, gas adsorption, nuclear magnetic resonance, and so on [12]. Pore development is generally affected by the reservoir mineral composition. Although different mineral compositions are affected by the same sedimentary environment during deposition, different pore structures are developed. On the other hand, in the process of diagenesis, pores, affected by mechanical compaction and cementation, will decrease, while diagenetic processes such as dissolution will make reservoir pores more developed [13].

Many scholars have studied the structure [14], sedimentation [15], rock [16], and minerals [17] in the Fengcheng Formation reservoir in Mahu Sag. In terms of reservoir pore structure characteristics, Chinese and foreign scholars have conducted many studies [18–20], but most of the studies focus on pore and fracture, and the research scale is singular, and few studies separate pore and fracture and multi-scale pore and fracture. On the basis of previous studies, this paper combines large-scale core characterization with small-scale characterization using scanning electron microscopy (SEM) and nuclear magnetic resonance (NMR) technology, and studies the reservoir structure of the Fengcheng Formation in Mahu Sag through the multi-scale characterization of pores and fractures separately, and expounds the genesis of pores and fractures to a certain extent, in order to enrich the reservoir research of the Fengcheng Formation in Mahu Sag. It contributes to the study of the energy storage pore structure of the Fengcheng Formation in Mahu Sag.

2. Geological Setting

The Junggar Basin is one of the large oil-bearing basins in western China, located in the eastern part of the Kazakhstan Plate, between the Altai Mountain and the Tianshan Mountain, with the western Junggar Mountains to the west and the foothills of the Beitar Mountains to the east [21,22]. Mahu Sag is located northwest of Junggar Basin, limited by the Wuxia-Kebai fault zone to the northwest, and adjacent to Yingxi Sag, the Sangequan uplift, Xiayan uplift, Dabasong uplift, and Zhongguai uplift in the east and southeast direction. It spreads in a NE–SW direction as a whole (Figure 1), with a total area of 4258 km^2, and is one of the hydrocarbon-generating sags with the highest degree of oil and gas enrichment in the Junggar Basin [23,24]. Mahu Sag was characterized by strong tectonic activity and tectonic inversion during the late Permian–Triassic period. It is a gentle monocline with a southeast dip, with steep characteristics in the west, slow characteristics in the east, thick characteristics in the west, and thin characteristics in the east. During the sedimentary period of the Fengcheng Formation in Mahu Sag, the sedimentary characteristics were controlled by climate change and volcanic activity, and mainly developed alkali-lacustrine facies. The Fengcheng Formation consists of the first member of the Fengcheng Formation (P$_1$f$_1$), the second member of the Fengcheng Formation (P$_1$f$_2$), and the third member of the Fengcheng Formation (P$_1$f$_3$) from the bottom up, with a thickness of about 800–1800 m and a burial depth of more than 4000 m. It is mainly deposited in lacustrine facies, mostly shale and occasionally siltstone interlayers, and the whole is dominated by dark fine-grained

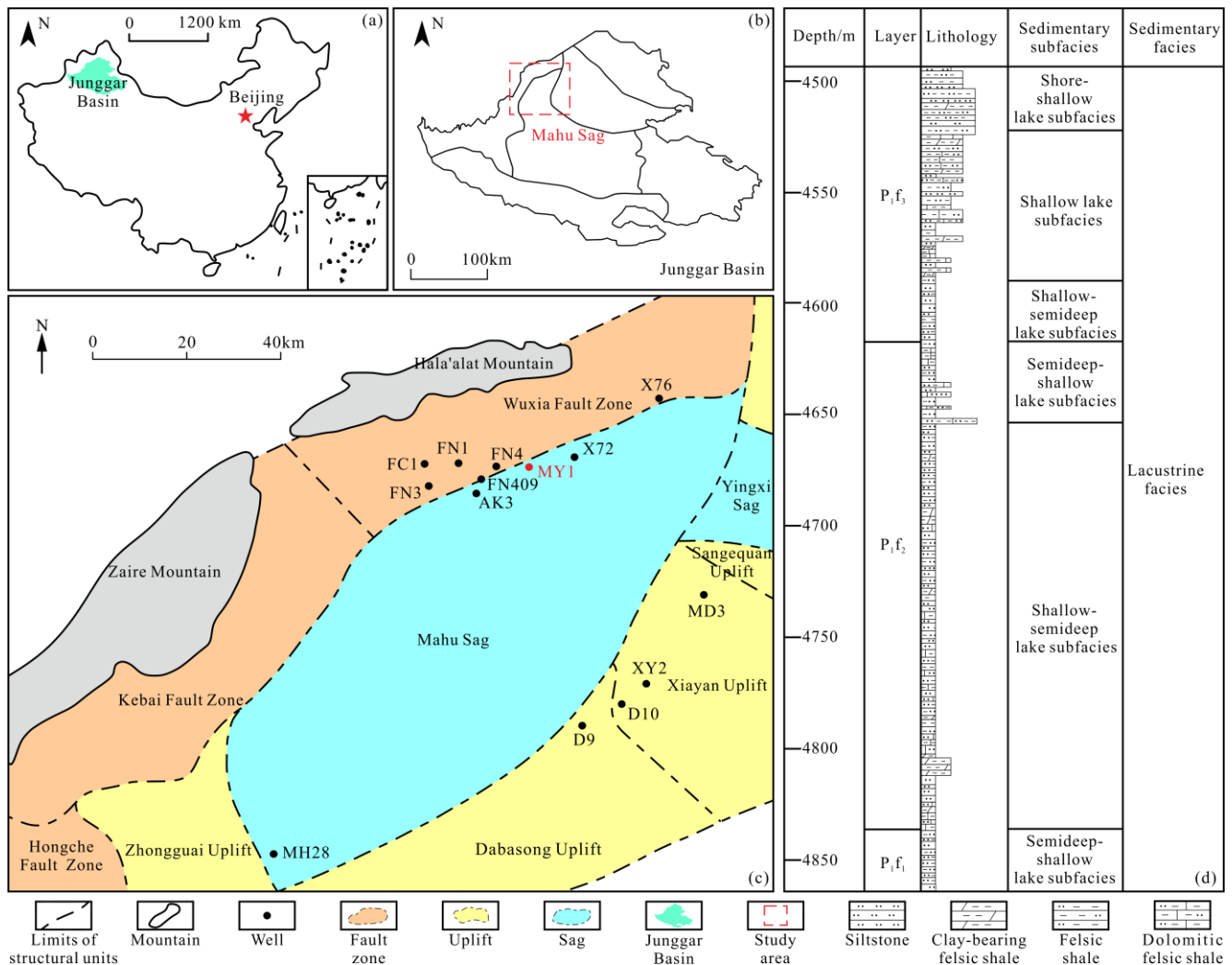sedimentary dolomitic shale and siliceous shale. It is the oldest alkali-lake source rocks in the world [25].

Figure 1. Schematic diagram of structural location of Mahu Sag in Junggar Basin. (**a**) The Junggar Basin and its location; (**b**) Location of the study area in the Junggar Basin; (**c**) Division of geological structural units in the research area; (**d**) MY1 well fengcheng Formation Lithological Column.

3. Samples and Methods

The samples selected in this study are from well Maye-1, Mahu Sag, Junggar Basin, with a depth of 4587–4858 m, belonging to the Fengcheng Formation interval. Well Maye-1 was drilled in 2019, with a maximum oil yield of 50.6 m^3 and an average daily oil output of 22.5 m^3, achieving a major breakthrough in the Fengcheng Formation shale oil [26]. Therefore, it is of great significance to study the Fengcheng Formation shale oil in Mahu Sag, Junggar Basin by selecting samples from the Fengcheng Formation of well Maye-1.

In this study, rock samples from different depths of well Maye-1 were first subjected to X-ray diffraction (XRD) experiments to analyze the mineral composition of the study area. The lithofacies were then classified based on grain size and mineral content. Two samples were selected from each lithofacies based on the lithofacies classification results, and were prepared separately for scanning electron microscopy (SEM) observation and nuclear magnetic resonance (NMR) experiments to investigate the development characteristics of pore–fracture systems in the Fengcheng Formation [27]. The specific procedures for each experiment are outlined below:

(1) The sample for the X-ray diffraction experiment needs to be ground into a powder sample; the particle size is 320 mesh, the total weight of the powder is about 5 g, and then the powder sample is used for the X-ray diffraction experiment;

(2) The samples used for SEM observation first need to be cut into a square with a side length of about 1 cm and a thin slice with a thickness of 2–3 mm. Next, the observation surface is polished by argon ion, and then, the pore and crack characteristics of the samples are observed by using field emission scanning electron microscopy (FE-SEM);

(3) The sample for the NMR experiment needs to be cut into a cylinder with a diameter of 2.5 cm and a height of 5 cm, and then the sample is saturated with water. The NMR experiment is carried out on the sample with a saturated water content.

Large-field splicing technology is a technology that first obtains multiple consecutive photos with large magnification and small field of view through FE-SEM, and then splices these high-precision small-field photos and assembles them together to obtain large-field high-precision images [28]. In this experiment, a GeminiSEM 300 FE-SEM instrument (Carl Zeiss AG, Oberkochen, Germany) was utilized to observe the pore and crack features on the surface of the sample. Subsequently, suitable regions were selected to obtain wide-field stitched images with dimensions of 500 μm × 500 μm and a maximum resolution of 10 nm. These images were then used to analyze the characteristics of pores and cracks in the corresponding samples.

The theoretical basis of the NMR technique is the NMR relaxation behavior of spin hydrogen nuclei (^{1}H) in the fluid contained in rocks under the action of the uniform distribution of a static magnetic field and radio frequency field. Based on this principle, the data of the full aperture inside the sample can be obtained from the measured results when the sample is saturated with water [29]. The experimental equipment used in this NMR analysis test is the RecCore-04 low magnetic field NMR rock sample analyzer (PetroChina Exploration & Development Research Institute, Beijing, China). The full aperture distribution characteristics of the samples were obtained and analyzed by using this instrument.

X-ray diffraction (XRD) is a commonly used material structure characterization method. Based on the scattering phenomenon of the interaction between the incident X-ray and the atoms or molecules in the crystal, the information about the crystal structure is obtained by measuring the intensity and angle of the scattered light, so as to obtain the mineral composition of the sample [30]. The experimental equipment used in this XRD test is the D8 ADVANCE X-ray diffractometer (Bruker, Billerica, MA, USA). Using this instrument, the whole rock analysis of the grinded powder samples is carried out to clarify the characteristics of the mineral components of the reservoir.

In addition, the fracture density on the core is calculated by using the core observation data, and the samples with relatively obvious characteristics of each lithology are selected for observation and analysis, and the macroscopic characteristics of pores and fractures of different lithologies are obtained.

4. Results

4.1. Petrological Characteristics

4.1.1. Mineral Composition Characteristics

During the sedimentation process, the mineral composition in different regions often varies due to influences such as sedimentary environment and diagenetic processes. These differences among minerals result in variations in the development of reservoir pore–fracture systems [31–33]. Therefore, clarifying the characteristics of the mineral composition is beneficial for gaining a deeper understanding of the factors influencing pore and fracture development in the study area. In this study, a total of 18 samples were selected for XRD experiments, and the results are shown in Table 1. The mineral composition of the Fengcheng Formation shale reservoir in the Mahu Depression is dominated by siliceous minerals and carbonate minerals (Figure 2a). The siliceous mineral content ranges from 34.9 to 90.0%, with an average of 62.2%, including quartz and feldspar. Among them, the

quartz content is between 14.2 and 58.7%, and the average is 34.1%; the feldspar content is between 11.3 and 47.4%, and the average is 28.2%, mainly plagioclase. The content of carbonate minerals is between 5.6 and 42.1%, with an average of 25.6%, mainly dolomite. Its content ranges from 3.1 to 42.1%, with an average of 19.7%. The content of clay minerals is low, ranging from 0.4 to 34.2%, with an average of only 5.0%. In addition, there are other minerals, mainly pyrite, between 0.9 and 12.9%, with an average of 7.2%.

Table 1. Mineral composition data of well Maye-1 based on XRD experiment.

| Depth (m)	Siliceous Minerals (%)			Carbonate Minerals (%)		Clay Minerals (%)	Others (%)
	Quartz	Potash Feldspar	Plagioclase Feldspar	Calcite	Dolomite		
4582.60	28.8	5.0	20.0	25.6	4.7	6.3	9.6
4587.92	35.6	5.1	12.4	5.1	6.7	34.2	0.9
4591.66	52.0	2.5	10.3	0.0	33.5	0.5	1.2
4633.48	56.5	4.6	17.3	0.9	14.9	4.2	1.6
4634.72	23.6	2.9	8.4	0.0	42.1	18.0	5.0
4690.85	39.7	6.0	21.9	1.1	18.5	2.3	10.5
4709.68	22.9	7.6	19.9	10.2	27.0	2.4	10.0
4720.30	41.6	3.3	18.2	4.5	25.7	0.8	5.9
4750.69	46.8	23.2	15.6	0.7	9.1	1.1	3.5
4758.44	14.5	28.1	13.1	2.3	29.5	0.4	12.1
4764.47	32.5	13.2	34.2	2.2	7.4	2.1	8.4
4776.66	33.8	3.3	32.5	4.8	12.9	1.3	11.4
4780.51	19.4	12.0	24.5	15.7	18.5	1.0	8.9
4783.10	58.7	21.7	9.6	2.5	3.1	0.5	3.9
4820.55	20.9	11.5	18.4	0.0	41.0	1.1	7.1
4829.15	35.4	6.2	19.6	0.0	27.2	3.9	7.7
4848.60	14.2	35.4	0.0	10.0	22.8	4.7	12.9
4858.41	36.2	10.4	8.8	21.3	9.8	5.1	8.4
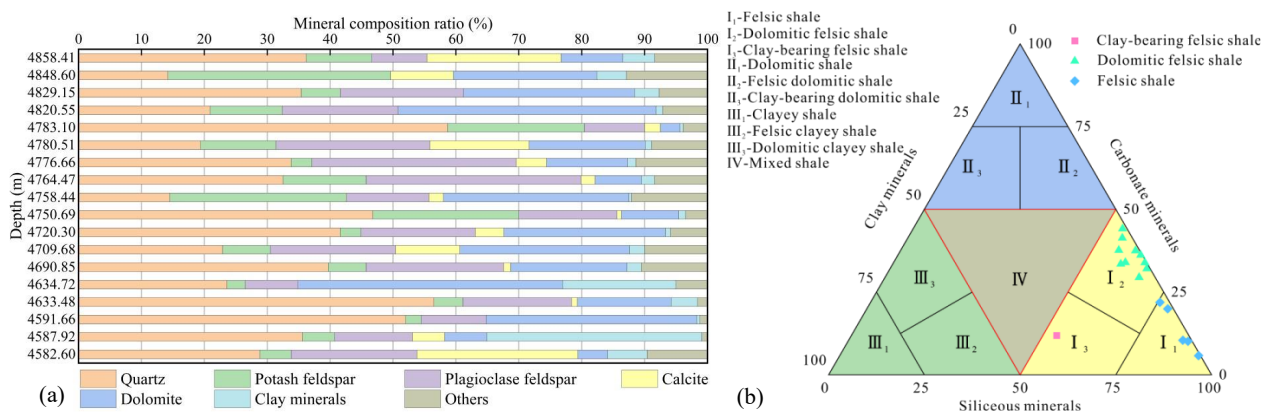
Figure 2. Image of petrological features. (**a**) Mineral composition ratio at different depths and (**b**) shale lithofacies division.

4.1.2. Lithofacies Division

Lithofacies represent the rocks or rock combinations formed in specific sedimentary environments, reflecting characteristics such as mineral composition and structure [11,34–36]. In the Mahu Depression, the Fengcheng Formation reservoirs are primarily composed of siliceous shale, with some intervals containing interbedded siltstone layers. Based on this geological background, we initially categorized the reservoirs into siltstone interlayers and shale formations based on grain size.

Subsequently, we use a ternary division method based on differences in mineral content, specifically whether the content of siliceous minerals, carbonate minerals, and clay minerals exceeds 50%, to classify the shale lithofacies [34]. The shale lithofacies are

categorized into four major types: felsic shale, dolomitic shale, clayey shale, and mixed shale. Based on the mineral content, the three major lithofacies excluding mixed shale are further subdivided. Felsic shale is subdivided into felsic shale, dolomitic felsic shale, and clay-bearing felsic shale based on the content of the other two minerals. Dolomitic shale is subdivided into dolomitic shale, felsic dolomitic shale, and clay-bearing dolomitic shale. Clayey shale is subdivided into clayey shale, felsic clayey shale, and dolomitic clayey shale (Figure 2b). In total, the shale is classified into four major categories and ten subcategories of lithofacies. Based on this criterion, the shale lithofacies in the Fengcheng Formation of the Mahu Depression primarily consist of felsic shale, dolomitic felsic shale, and clay-bearing felsic shale. Combined with the interbedded siltstone interlayers, the lithofacies in the study area are ultimately classified into these four types.

4.2. Pore Development Characteristics

4.2.1. Macroscopic Pore Characteristics

The typical core samples of each lithology in the study area were selected for observation and description, and the results are shown in Figure 3. From the core, the pores of each lithology are dominated by solution pores, among which, the pores in the felsic shale are mostly filled with alkaline minerals, in the form of slits, with a width of about 1–4 mm and a length of 1–1.5 cm. The pore development of dolomitic felsic shale is similar to that of felsic shale, with large pores, a large pore size and span, and an irregular pore shape, and the scale is developed at the scale of 1 mm–1 cm. The pores of clay-bearing felsic shale are poorly developed, with small pore scales, mostly round and oval shapes, with diameters of about 1–4 mm, and mostly filled with clay minerals. Siltstone interlayer pores are more developed; the single scale is small, the shape is mostly round and oval, and the diameter is basically between 1 and 6 mm.
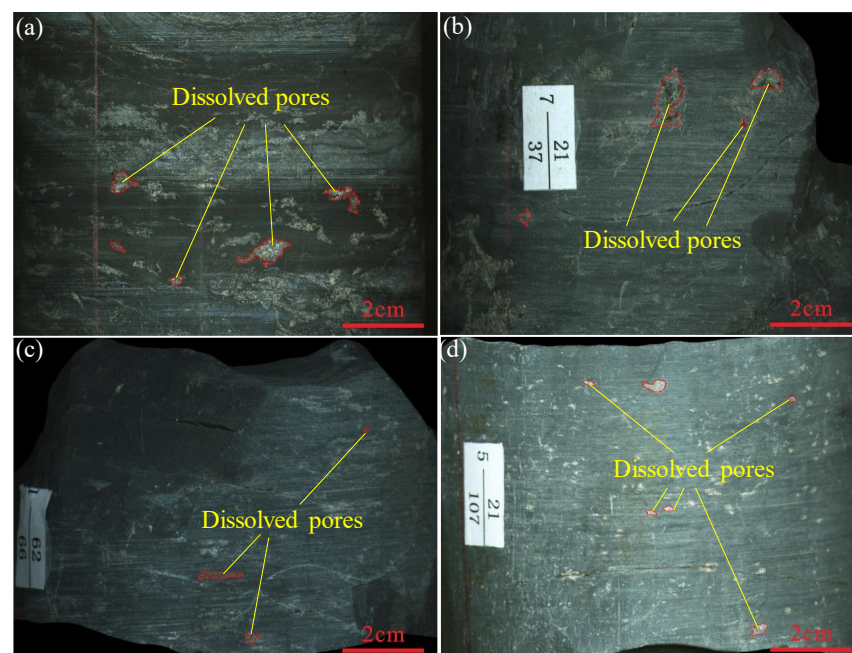

Figure 3. Core map of each lithology. (**a**) Felsic shale, 4691.21 m; (**b**) dolomitic felsic shale, 4648.65 m; (**c**) clay-bearing felsic shale, 4587.25 m; and (**d**) siltstone interlayers, 4623.91 m.

4.2.2. Microscopic Pore Characteristics

In this study, samples from the designated study area underwent argon ion polishing before being observed using FE-SEM. The pores were categorized into intra-, intergranular, and organic based on their location and origin. In the study area, predominant pore types included intra- and intergranular dissolved pores, whereas organic pores were less prevalent.

As shown in Figure 4, on the whole, the pores of felsic shale are well-developed, most of which are intergranular pores, with a small number of intra-granular pores. Most of them are triangular, circular, and slit types. The width of the slit pores is 10–500 nm and the length is basically 100–2000 nm, while the size of the triangular and circular pores is smaller, ranging from 5 to 500 nm. On the whole, the pores of dolomitic felsic shale are well-developed, and the pore types are mainly intergranular pores and intra-granular pores, among which the intergranular pores are mostly triangular or polygonal, with scales ranging from 50 to 500 nm, while the intra-granular pores are mostly round or oval, with scales varying from 20 to 200 nm. On the whole, the pore development of clay-bearing felsic shale is worse than that of felsic shale and dolomitic felsic shale. Among them, the pore width of slits is only 5–100 nm and the length is 10–300 nm. Most of them are intergranular pores of clay minerals, and there are also intragranular dissolved pores, which are oval and round in shape and vary in diameter, from 50 to 350 nm. On the whole, the pore development of siltstone interlayers is obviously better than that of the other three lithology samples. The pores are mainly intergranular pores, and their morphology varies according to the different mineral particle edges, such as triangles and polygons. The scale span is large, and the side length is 100–4000 nm, which has the best reservoir ability.
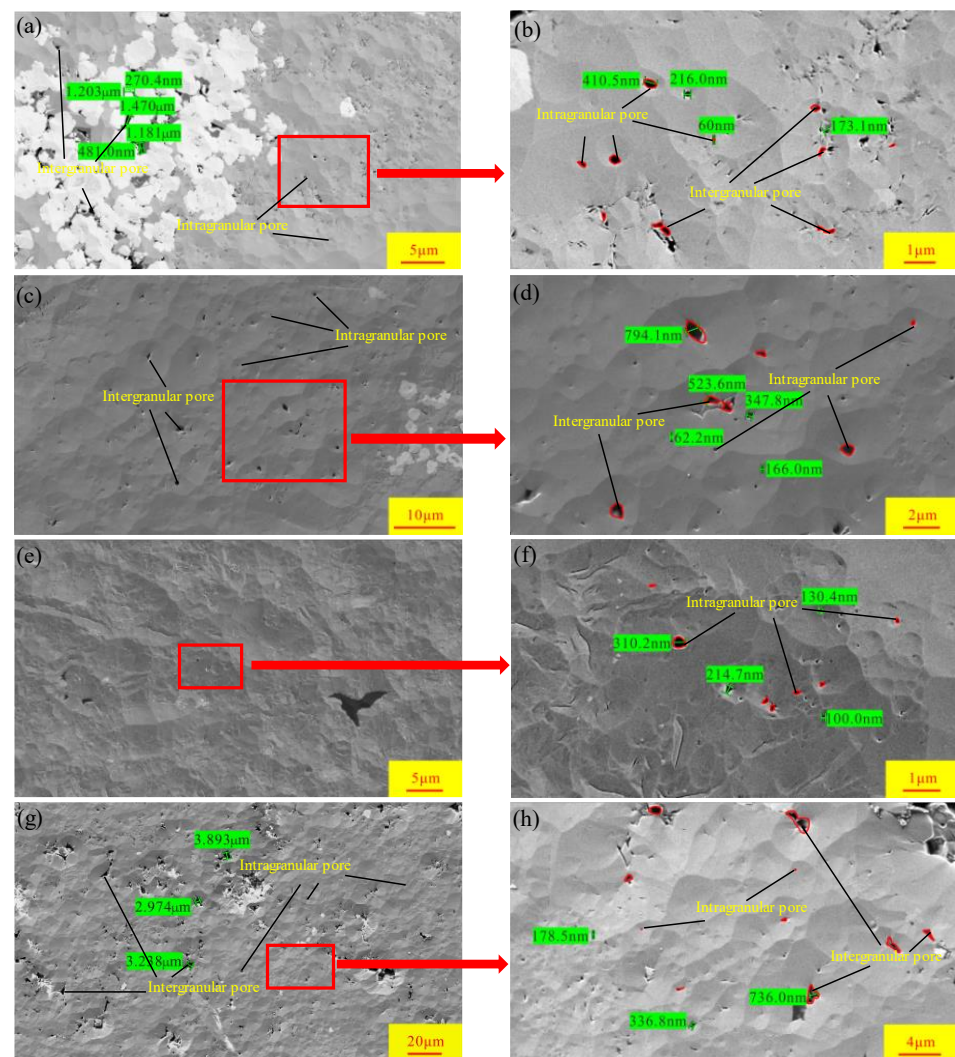

Figure 4. Pores in SEM of each lithology. (**a**) Felsic shale, 4755.67 m; (**b**) felsic shale (Part); (**c**) dolomitic felsic shale, 4857.57 m; (**d**) dolomitic felsic shale (Part); (**e**) clay-bearing felsic shale, 4587.92 m; (**f**) clay-bearing felsic shale (Part); (**g**) siltstone interlayers, 4635.30 m; and (**h**) siltstone interlayers (Part).

4.3. Fracture Development Characteristics

4.3.1. Macroscopic Fracture Characteristics

From the core results, all the four lithologies have fracture development, but the development degree is different according to the different lithology. As shown in Figure 5, the macro-fractures of felsic shale have the best development, most of which are structural fractures and dissolution fractures, etc., but most of them are filled by alkaline minerals, and the fracture width is small, with an average width of less than 1 mm. The second is the siltstone interlayers, and the macro-fractures are well-developed, mostly structural fractures, contraction fractures, etc., with an average width of 2.21 mm. Macroscopically, there are many types of fractures such as multi-developed interlayer fractures and structural fractures, and their widths are medium, with an average width of 1.78 mm. The macro-fractures of clay-bearing felsic shale are the least developed, and most of the types are structural fractures and dissolution fractures, etc., which are mostly developed around mineral particles and filled with clay minerals. The fracture width is small, and the average fracture width is less than 1 mm.
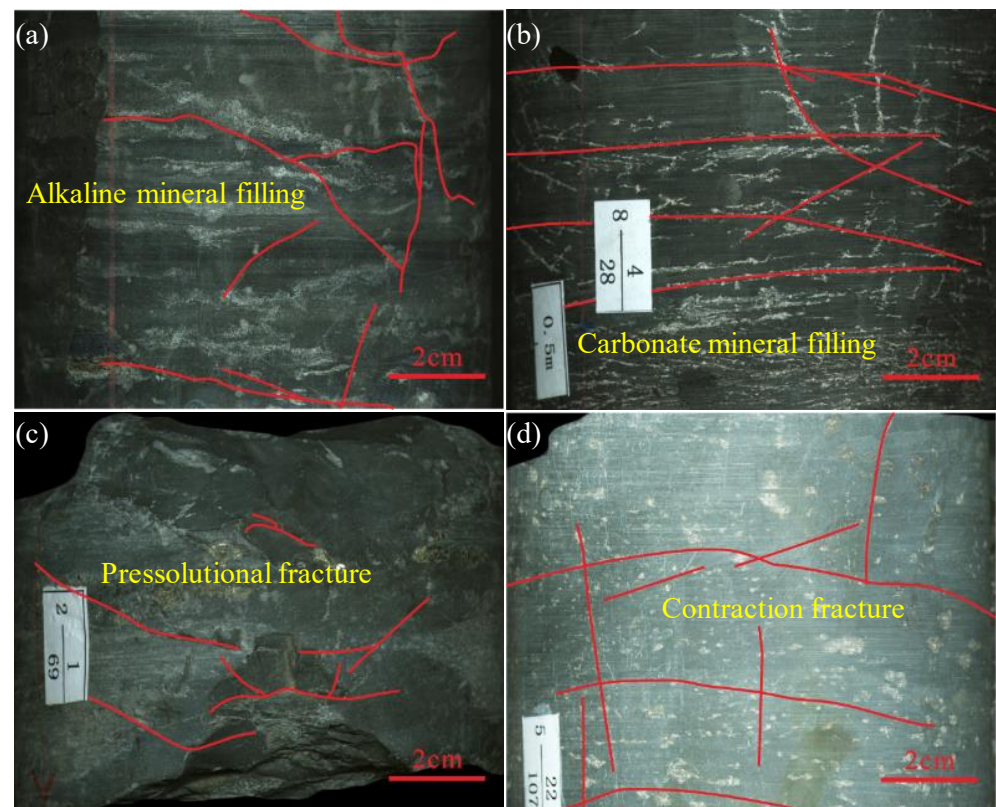

Figure 5. The core fractures of each lithology(red line is fractures). (**a**) Felsic shale, 4691.43 m; (**b**) dolomitic felsic shale, 4658.23 m; (**c**) clay-bearing felsic shale, 4587.95 m; and (**d**) siltstone interlayers, 4624.10 m.

The macroscopic fracture density of the cores of four lithology types in well Maye-1 is calculated through core observation. As shown in Figure 6, the macroscopic fracture density of felsic shale is the highest, followed by siltstone interlayers, and the fracture density of clay-bearing felsic shale is the lowest. Therefore, from a macroscopic perspective, the fluidity of felsic shale is the best, while the connectivity of clay-bearing felsic shale is the worst.

The fracture development of the four lithology types is mainly affected by stratigraphic tectonic movement, in which the proportion of brittle minerals in the dolomitic felsic shale increases due to the increase in the content of carbonate rock, making fractures more likely to occur. In other lithologies, multiple small fractures are connected together, showing large

fractures in length and width. The brittle minerals of felsic shale are poor, and its fractures are dominated by a large number of smaller fractures. Because of the poor brittleness of clay minerals, clay-bearing felsic shale will fill cracks, so its fracture development is the worst and the number of cracks is the least. The fracture development of siltstone interlayers is better, which is related to the properties of siltstone interlayers themselves, with a larger grain size and higher brittleness.
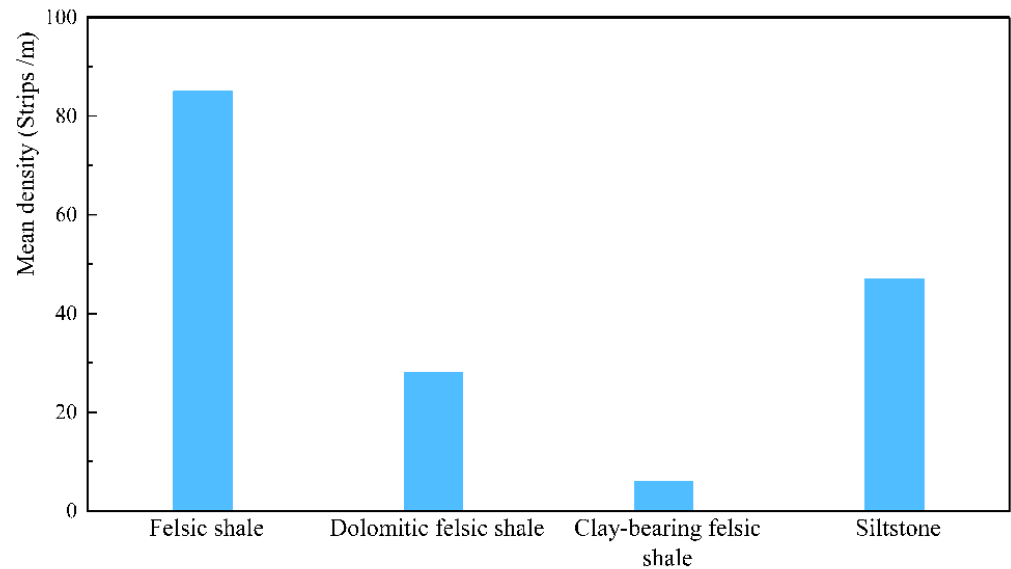
Figure 6. Statistical chart of core fracture density.

4.3.2. Microscopic Fracture Characteristics

At the microscopic level, the development of each lithologic fracture is different from that of the macroscopic fracture. As shown in Figure 7, intergranular fractures and suture lines of felsic shale are developed, with good connectivity and fracture widths ranging from 10 to 200 nm, which are good seepage channels. The fractures developed in the dolomitic felsic shale are mainly particle edge fractures, which communicate with the dissolution pores, and the suture lines are relatively developed, with widths ranging from 30 nm to 300 nm. The length span of the fractures is large, with the short fractures only 500 nm and the long fractures up to 18 μm. The fracture types of clay-bearing felsic shale are mainly clay mineral shrinkage fractures, and well-developed fractures are occasionally seen. The width of fractures is between 10 and 200 nm, and the fractures are relatively isolated with few communication pores. The fracture connectivity is the worst among the four lithologies. The structural fractures of siltstone interlayers often develop along the edge of mineral particles, and the dissolution pores are mainly communicated through the mineral edge fractures, with the width of the fractures between 20 and 200 nm. The fractures have good connectivity.
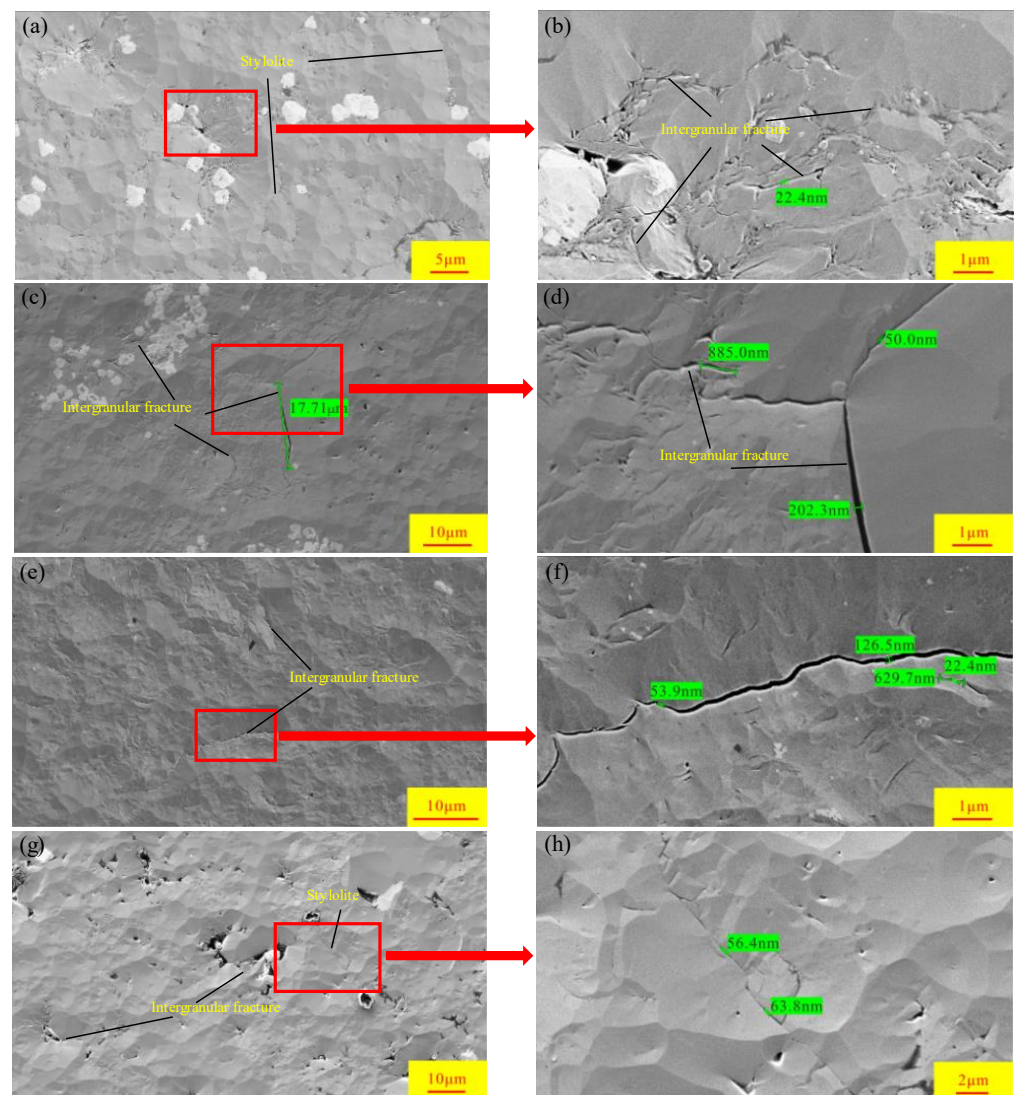
Figure 7. Fractures in SEM of each lithology. (**a**) Felsic shale, 4755.67 m; (**b**) felsic shale (Part); (**c**) dolomitic felsic shale, 4857.57 m; (**d**) dolomitic felsic shale (Part); (**e**) clay-bearing felsic shale, 4587.92 m; (**f**) clay-bearing felsic shale (Part); (**g**) siltstone interlayers, 4635.30 m; and (**h**) siltstone interlayers (Part).

5. Discussion

5.1. Joint Characterization of Pore–Fracture

NMR is a technique that reflects the pore size of a sample by measuring the relaxation time of the fluid in the pore. The T_2 spectrum, which is measured when the rock is saturated with water, is the characteristic of the pore development inside the rock sample. In this study, NMR experiments were carried out on the water-saturated samples of four lithologies, and their relaxation time and signal strength were converted to obtain the relationship between the sample pore size and pore volume.

As shown in Figure 8, the NMR curves of different lithologies are significantly different. Among the four lithologies, siltstone interlayers have the widest pore distribution range, with double peaks visible. The main development range is 10–800 nm, the pore volume is the largest, and the pore size is concentrated at the pore size above 100 nm, indicating that the pores above 100 nm are the main ones. Among the four lithologies, it has the highest porosity and the best reservoir capacity. Secondly, dolomitic felsic shale has obvious bi-peak characteristics, which are in the pore size range of 5–15 nm and 200–500 nm, respectively.

Moreover, the NMR curve in the small pore size range has a higher peak and larger pore volume, indicating that the main pore size of dolomitic felsic shale is in the pore size range of 5–15 nm, and the porosity is lower than that of siltstone interlayers but higher than that of other lithologies. It has second-order storage capacity, and the small pore size is the main storage space. Felsic shale can also show double peak characteristics, but its pore volume is smaller than that of dolomitic felsic shale and siltstone interlayers, and its porosity is worse. The pore size range is mainly 5–400 nm, and pores with a smaller pore size are more developed from the perspective of pore volume. Only one peak is observed for clay-bearing felsic shale and it is located in the pore size range of 5–50 nm; its development pores are very small, the porosity is the worst, and the reservoir capacity is also the worst.

From the overall distribution of the image, siltstone interlayers, dolomitic felsic shale, and felsic shale have visible peaks on the right side of the image, indicating that the internal fluid relaxation time of these three types of samples is relatively long, and the fluid is free. This state means that there may be cracks, large aperture pores in the sample, and there are more movable fluids. Among the three, the right peak of siltstone interlayers is the highest, followed by dolomitic felsic shale, indicating that siltstone interlayer fractures are the most developed, followed by dolomitic felsic shale fractures, and felsic shale fractures are the worst. The right peak is not observed for the clay-bearing felsic shale, so its cracks are almost not developed.
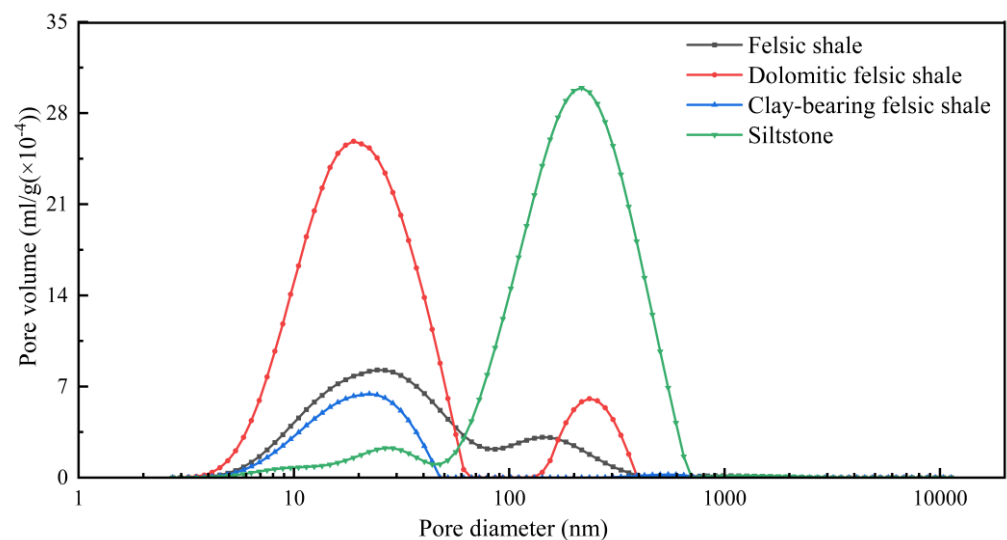

Figure 8. NMR curves of each lithology.

5.2. Multi-Scale Coupling Development Model of Pores and Fractures

In this study, macroscopic pores and fractures were studied at the centimeter scale through drilling core research, and then microscopic pores and fractures were studied at the micro and nanoscale through SEM (Figure 9). The results show that the reservoir space of Fengcheng Formation shale has multi-scale and multi-type characteristics.

Then, through the quantitative calculation of the pores and fractures of the samples of four lithologies, the respective porosity of the fractures and the pores of each lithology were calculated, the contribution rate of the fractures was calculated according to the results, and the pore and fracture development characteristics of the four lithologic reservoirs in the Fengcheng Formation were obtained. The results are shown in Table 2.
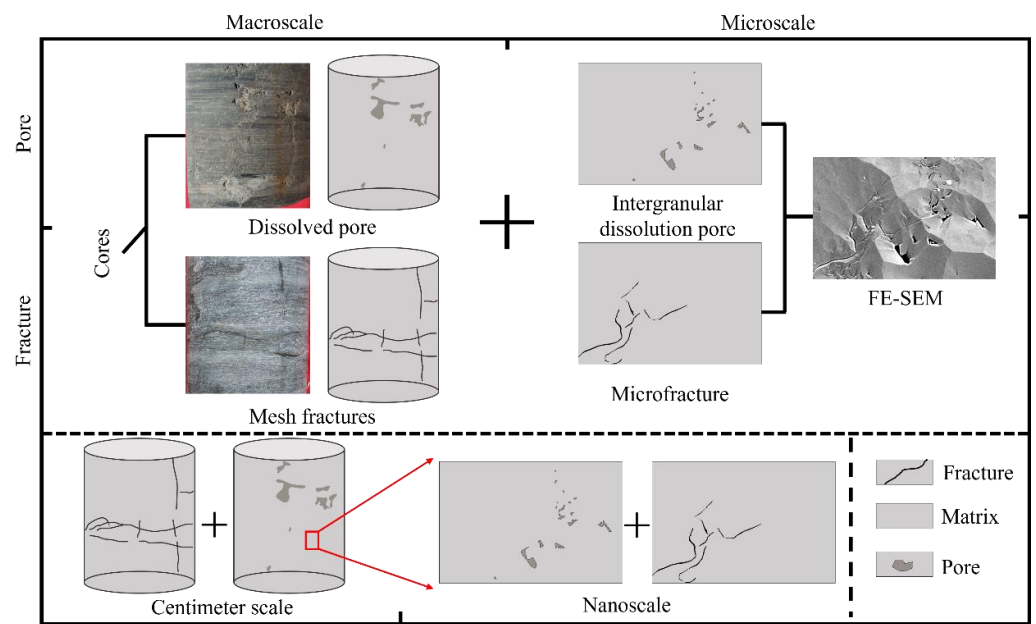
Figure 9. Multi-scale coupling development model of pores and fractures.

Table 2. Porosity statistics of each lithology.

Lithology	Porosity%	Fracture Porosity%	Fracture Contribution Rate %	Total Porosity %
Felsic shale	3.85	1.48	27.76	5.33
Dolomitic felsic shale	2.57	10.37	80.14	12.94
Clay-bearing felsic shale	1.12	1.5	57.25	2.62
Siltstone interlayers	6.69	7.2	51.84	13.89

It can be clearly seen from Table 2 that the overall total porosity of siltstone interlayers is the highest, and its pore and fracture development is obviously better than that of the shale lithology. The development of pores and fractures is relatively balanced, and the porosity degree of the two is basically the same. Among the three shale types, the porosity of dolomitic felsic shale is the best, and its pore development is at the medium level among the three lithologies, only 2.57%. However, its fracture development is particularly good, and the fracture porosity is the highest, even exceeding the sandstone fracture porosity, reaching 10.37%. The porosity development of felsic shale is superior to that of the other three lithologies, reaching 3.85%, showing that the porosity development is superior to the fracture development in the pore structure. Although the fracture development of clay-bearing felsic shale is very close to that of felsic shale, the pore development is very poor, and the porosity is only 1.12%. From the perspective of pore structure, the development of pores and fractures is relatively balanced.

The shale of the Fengcheng Formation in Mahu is dominated by felsic shale. Therefore, in this study, when analyzing the differences in the pore and fracture development of the three types of shale, felsic shale is taken as the benchmark. It can be found that when the clay content is high, the fracture porosity is basically similar to that of felsic shale, but the porosity decreases a lot. This may be due to the increase in clay content, which leads to the filling of some pores in the shale by clay minerals. Therefore, the fracture contribution rate of the shale is much higher than that of the feldspar sheet, and even exceeds that of the siltstone interlayers, reaching 57.25%. Compared with that of felsic shale, the porosity of dolomitic felsic shale decreases somewhat, but the fracture porosity far exceeds it. This may be due to the increased brittleness of shale caused by the increase in the dolomite content, which makes it more likely to fracture and form fractures when subjected to tectonic movement or external pressure. Therefore, the contribution rate of the fracture is much higher than that of other

lithologies, up to 80.14%. Compared with siltstone interlayers, the development of fractures and pores in shale is much lower than that of siltstone interlayers due to its formation factors. These conclusions are basically consistent with the previous NMR measurement results, and the two are mutually corroborated, indicating the reliability of the research.

In conclusion, it can be inferred that the development of pores and fractures within siltstone interlayers is the best reservoir in the Fengcheng Formation reservoir in Mahu Sag. The pores and fractures of siltstone interlayers are more balanced and have the largest porosity. The reservoir potential of dolomitic felsic shale is superior, with fractures dominating both its primary storage capacity and seepage pathways.

5.3. Mechanism of Aperture Development

By studying the mechanism of pore development, we can understand the influencing factors of pore formation and clarify the formation conditions of pore formation, so as to have a deeper understanding of pore development. The pore and fissure development of the Fengcheng Formation in Mahu Sag is mainly influenced by sedimentary tectonic movement and diagenesis in the study area.

5.3.1. Sedimentary Tectonic Factors

Sedimentation and structure are the main reasons for the initial formation and burial depth of strata [37]. Different sedimentary environments and different material sources have great influence on the formation of reservoirs. By clarifying the sedimentary environment, we can understand the sedimentary types in the sedimentary period, so as to clarify the reservoir lithology in the study area, and divide the shale and sandstone interlayers. By clarifying the material sources, we can understand the mineral types and contents of the constituent rocks, and make a more detailed division of the shale types. In addition, different minerals have different physical properties, which will have different effects on the formation of pores [38,39].

The Fengcheng Formation in Mahu Sag mainly develops three subfacies deposits from bottom to top: semi-deep lacustrine subfacies, shallow lacustrine subfacies, and lakeshore subfacies, and mainly develops felsic shale. In addition, there are well-sorted siltstone interlayers in the shallow lake subphase. In the water environment of semi-deep lacustrine subfacies and shallow lacustrine subfacies, carbonate minerals are well preserved, so the content of carbonate minerals is relatively high in some strata. Besides felsic shale, dolomitic felsic shale also develops. But in semi-deep lacustrine subfacies, massive structures (Figure 10a) and horizontal bedding (Figure 10d) are mainly developed. In shallow lacustrine subfacies, the laminae (Figure 10f), dolomite bands (Figure 10e), and siltstone interlayers with anti-rhythmic bedding from fine to coarse (Figure 10c) are mainly developed. Due to the proximity of lakeshore subfacies to the land, carbonate minerals are susceptible to weathering and terrigenous clastic minerals are abundant; in addition to felsic shale, clay-bearing felsic shale is also developed, and the structure is mainly dominated by wavy bedding (Figure 10b).

The mineral composition of shale has a certain influence on the pore and fracture development of shale. As shown in Figure 11, the relationship between various mineral contents and porosity was determined with plotting envelope curves, and the influence of different minerals on porosity was analyzed. Siliceous and carbonate minerals are both brittle minerals; the higher their content, the larger the porosity and the more developed the pore structure. A comparative analysis of Figure 11a,b reveals that, relatively speaking, carbonate minerals exhibit a higher correlation with porosity, with a steeper slope, indicating a stronger positive effect on pore development. An increase in the carbonate mineral content favors pore formation, consistent with the conclusions drawn from the comparison of porosity between different lithofacies in the previous section. On the other hand, as depicted in Figure 11c, the envelope curve slopes downward, indicating that clay minerals have an inhibitory effect on pore formation. A higher clay mineral content corresponds to poorer pore development, aligning with the findings obtained earlier.
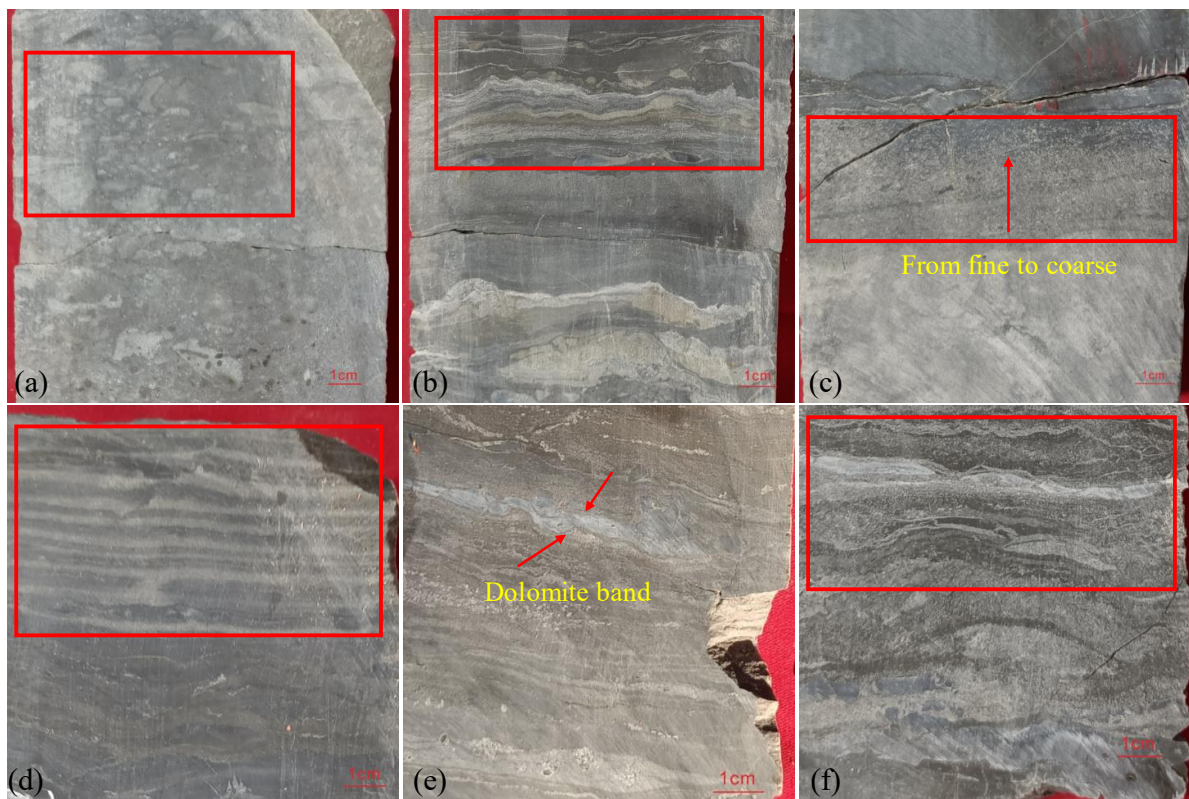
Figure 10. Schematic diagram of sedimentary structure. (**a**) Blocky structure; (**b**) wavy bedding; (**c**) anti-rhythmic bedding; (**d**) horizontal bedding; (**e**) dolomite band; and (**f**) dolomite layers.
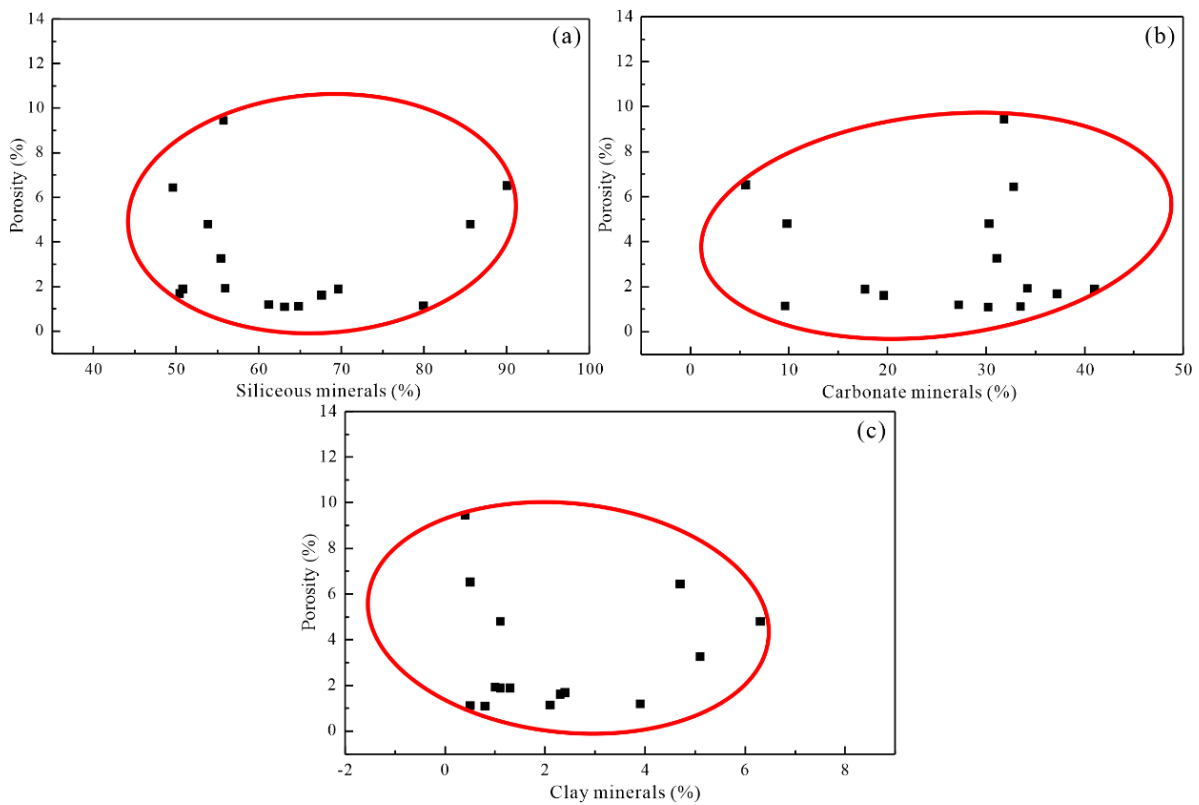

Figure 11. Relationship between minerals and porosity. (**a**) Relationship between porosity and siliceous minerals; (**b**) Relationship between porosity and carbonate minerals; (**c**) Relationship between porosity and clay minerals.

In addition to the influence of different mineral components caused by provenance on the development of pores and fractures, the different pressure caused by the buried depth of sedimentary strata will also have a certain impact on the development of pores and fractures. Affected by the formation pressure, with the increase of burial depth, the porosity of the reservoir gradually decreases, and the occasional increase in porosity is due to the increase in porosity caused by the dissolution of diagenesis.

The Mahu Sag area was subjected to strong tectonic movements such as extrusion, uplift, and denudation, which were conducive to the formation of faults and fractures in the reservoir [40], but later, diagenesis resulted in some fractures being filled with alkaline minerals or clay minerals. The formation of these faults and fractures improves the reservoir's physical properties and provides the channels for vertical and lateral oil and gas transport.

5.3.2. Diagenesis

Diagenesis determines the evolution of the reservoir's pore structure under buried depth conditions and has a direct control on the final physical properties of the reservoir [41]. The diagenesis types of the Fengcheng Formation reservoir are various, and mainly include compaction, pressure dissolution, dissolution, and metasomatism. Among them, the compaction effect is relatively strong, and with the increase in buried depth, the particles are arranged more closely, resulting in the surface fracture of some rigid particles to form fractures (Figure 12a). Pressure dissolution is mainly developed at the joints of rock particles, and suture structures can be seen in some areas (Figure 12b). The dissolution mainly develops inside the cement particles and between feldspar, quartz, and carbonate mineral particles, forming intergranular dissolution pores, intragranular dissolution pores, and dissolution fractures (Figure 12c). Metasomatism mainly involves the replacement of clay minerals by calcite, authigenic minerals by quartz, and carbonate minerals by siliceous minerals (Figure 12d). These diagenetic processes play a very important role in the development of reservoir pores, and directly or indirectly lead to the formation of micro-pores and micro-fractures.
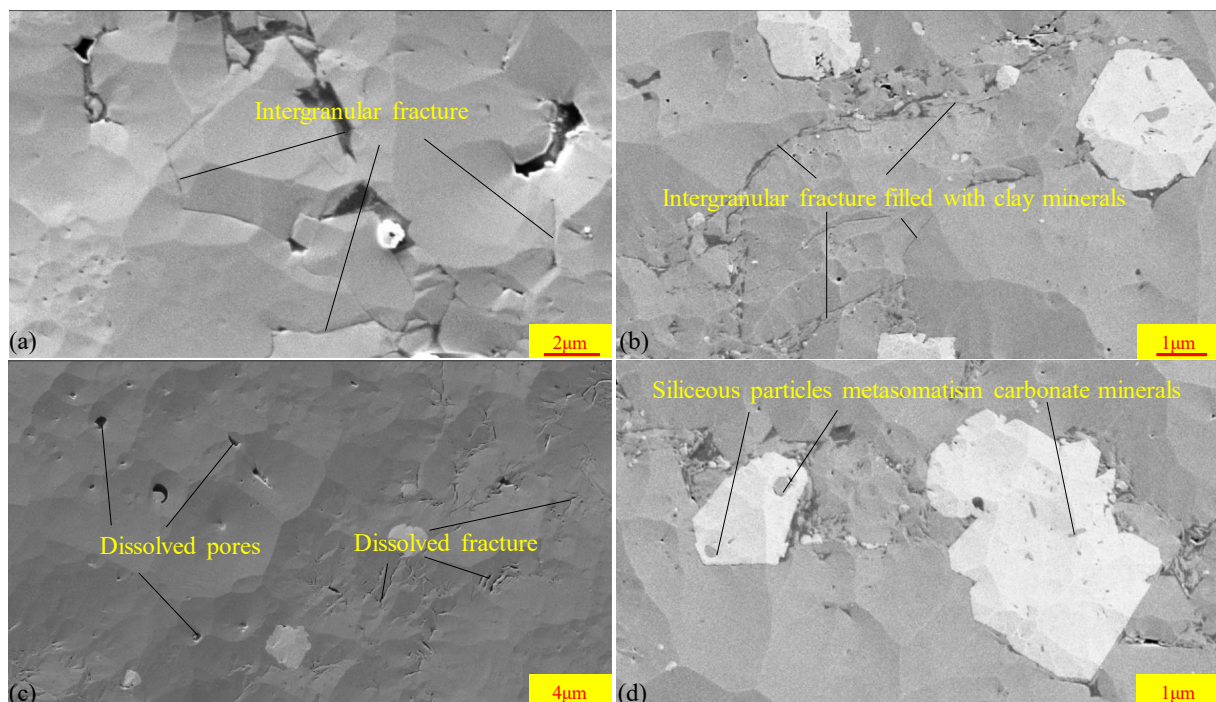

Figure 12. Schematic diagram of diagenesis. (**a**) Compaction; (**b**) pressure solution; (**c**) dissolution; and (**d**) metasomatism.

As shown in Figure 13, Figure 13a is the variation curve of porosity with depth. The deeper the depth, the higher the pressure temperature and the stronger the compaction effect, so the overall porosity increases with the depth. However, due to the late diagenetic processes of dissolution and metasomatism, some minerals in the rock reservoir are metasomatized or dissolved, so that the deep reservoir with low porosity has high porosity. Among them, corrosion greatly promoted the formation of pores. As shown in b and c in Figure 13, the images were SEM images of positions with high porosity in deep strata, from which it could be seen that the development of pores was dominated by corrosion pores and fractures, and the matrix between mineral particles was mostly formed by corrosion.
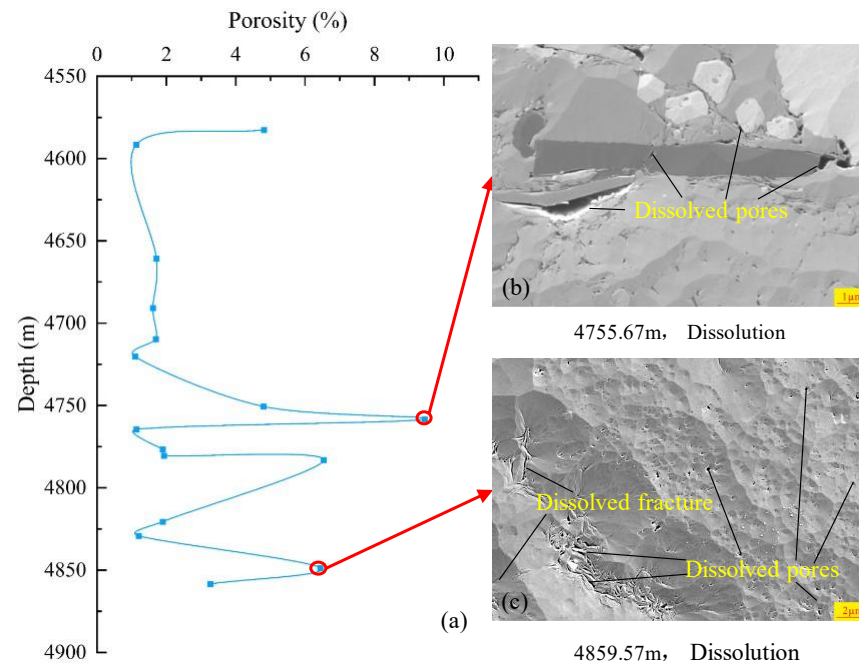
Figure 13. Porosity variation with depth and diagenesis diagram. (**a**) Diagram of porosity variation with depth; (**b**) 4755.67 m, Dissolution; (**c**) 4859.57 m, Dissolution.

To sum up, diagenesis has a great influence on the development of pores and fractures. The main observation is that the porosity of the strata is reduced by early compaction, and the metasomatism and dissolution in the compacted strata promote the development of pores and fractures in the later period, so that the porosity of the strata begins to increase. However, due to the different mineral composition of the reservoir in the study area, the pores of plastic minerals such as clay minerals, after being compacted, are mostly of the narrow-slit type, while the pores of brittle mineral particles that can withstand the pressure will retain the original appearance of the solution pores, showing round, oval, or polygon shapes. If the pressure is too large, fractures will occur, resulting in the formation of structural fractures and other fractures, thus affecting the development of reservoir pores.

6. Conclusions

1. Based on the mineral composition and grain size variation of the Fengcheng Formation reservoir in the Mahu Depression, four lithofacies were delineated, each exhibiting distinct pore and fracture development characteristics. Siltstone interlayers displayed the most extensive porosity development, characterized by fewer macropores but abundant micro-pores, with sizes ranging from 100 nm to 4000 nm, primarily intergranular, followed by felsic shale, while clay-bearing felsic shale exhibited the poorest development, dominated by interparticle pores with the smallest pore diameters. Dolomitic felsic shale featured the most developed fractures, predominantly comprising interbedded and structural fractures, with a fracture porosity reaching 10.37%, which was significantly higher than other lithofacies. Siltstone interlayers ranked next,

with felsic shale and clay-bearing felsic shale exhibiting similar fracture development patterns, albeit with lower macroscopic fracture densities; the poorest connectivity was observed in clay-bearing felsic shale.

2. Among the four lithofacies, siltstone interlayers exhibited the most favorable overall pore and fracture development conditions, with pore and fracture porosities showing little discrepancy but relatively high values overall. In contrast, clay-bearing felsic shale displayed the poorest overall pore and fracture development. Dolomitic felsic shale featured the highest proportion of fractures in its pore–fracture system, boasting superior connectivity, whereas felsic shale exhibited the least developed internal fractures and contributed the lowest fracture porosity. Overall, siltstone interlayers were deemed the most favorable reservoir among the four lithofacies, with dolomitic felsic shale showing distinct advantages among the three shale types.

3. The development of pores and fractures is primarily influenced by sedimentary and diagenetic factors. Sedimentation primarily occurred in semi-deep lake, shallow lake, and lakeshore subfacies. A higher carbonate mineral content during sedimentation resulted in increased shale brittleness and the enhanced propensity for fracture formation. Structural processes mainly led to the formation of large-scale macroscopic fractures, while diagenetic processes, including compaction, pressure solution, dissolution, and replacement, played a crucial role in pore formation, which his closely associated with pore genesis.

References

1. Xu, C.C.; Zou, W.H.; Yang, Y.M.; Duan, Y.; Shen, Y.; Luo, B.; Ni, C.; Fu, X.D.; Zhang, J.Y. Status and Prospects of Deep Oil and Gas Resources Exploration and Development Onshore China. *J. Nat. Gas Geosci.* **2018**, *3*, 11–24. [CrossRef]
2. Tong, X.G.; Zhang, G.Y.; Wang, Z.M.; Wen, Z.X.; Tian, Z.J.; Wang, H.J.; Ma, F.; Wu, Y.P. Distribution and Potential of Global Oil and Gas Resources. *Pet. Explor. Dev.* **2018**, *45*, 779–789. [CrossRef]
3. Wang, H.J.; Ma, F.; Tong, X.G.; Liu, Z.D.; Zhang, X.S.; Wu, Z.Z.; Li, D.H.; Wang, B.; Xie, Y.F.; Yang, L.Y. Assessment of Global Unconventional Oil and Gas Resources. *Pet. Explor. Dev.* **2016**, *43*, 925–940. [CrossRef]
4. Bai, L.N.; Huang, W.B.; Qin, J.; Zhang, Z.B.; Ba, Z.C.; Bai, Z.H.; Guo, Y.B.; Li, H. Genesis and Microscopic Characteristics of Tight Reservoirs in the Fengcheng Formation, at the Southern Margin of the Mahu Sag. *Energy Geosci.* **2023**, *4*, 100162. [CrossRef]
5. Lv, J.H.; Jiang, F.J.; Hu, T.; Zhang, C.X.; Huang, R.D.; Hu, M.L.; Xue, J.; Huang, L.L.; Wu, Y.P. Control of Complex Lithofacies on the Shale Oil Potential in Ancient Alkaline Lacustrine Basins: The Fengcheng Formation, Mahu Sag, Junggar Basin. *Geoenergy Sci. Eng.* **2023**, *224*, 211501. [CrossRef]

6.   Zheng, Y.J.; Liao, Y.H.; Wang, J.; Xiong, Y.Q.; Wang, Y.P.; Peng, P.A. Factors Controlling the Heterogeneity of Shale Pore Structure and Shale Gas Production of the Wufeng–longmaxi Shales in the Dingshan Plunging Anticline of the Sichuan Basin, China. *Int. J. Coal Geol.* **2024**, *282*, 104434. [CrossRef]

7.   Zhang, C.J.; Hu, Q.H.; Yang, S.Y.; Zhang, T.; Dong, M.Z.; Sang, Q.; Ke, Y.B.; Jiang, H.Q.; Jin, Z.J. Hierarchical Cluster and Principal Component Analyses of Multi-scale Pore Structure and Shale Components in the Upper Triassic Chang 7 Member in the Ordos Basin of Northern China. *J. Asian Earth Sci.* **2024**, *261*, 106001. [CrossRef]

8.   Huang, Y.Y.; Wang, G.W.; Zhang, Y.; Xi, J.H.; Huang, L.L.; Wang, S.; Zhang, Y.L.; Lai, J.; Jiang, C.Z. Logging Evaluation of Pore Structure and Reservoir Quality in Shale Oil Reservoir: The Fengcheng Formation in Mahu Sag, Junggar Basin, China. *Mar. Pet. Geol.* **2023**, *156*, 106454. [CrossRef]

9.   Dong, S.Q.; Zeng, L.B.; Du, X.Y.; He, J.; Sun, F.T. Lithofacies identification in carbonate reservoirs by multiple kernel Fisher discriminant analysis using conventional well logs: A case study in A oilfield, Zagros Basin, Iraq. *J. Pet. Sci. Eng.* **2022**, *210*, 110081. [CrossRef]

10. Pang, X.J.; Wang, G.W.; Kuang, L.C.; Zhao, F.; Li, C.L.; Wang, C.Y.; Zhang, M.; Lai, J. Lamellation fractures in shale oil reservoirs: Recognition, prediction and their influence on oil enrichment. *Mar. Pet. Geol.* **2023**, *148*, 106032. [CrossRef]

11. He, X.B.; Luo, Q.; Jiang, Z.X.; Qiu, Z.X.; Luo, J.C.; Li, Y.Y.; Deng, Y. Control of complex lithofacies on the shale oil potential in saline lacustrine basins of the Jimsar Sag, NW China: Coupling mechanisms and conceptual models. *J. Asian Earth Sci.* **2024**, *266*, 106135. [CrossRef]

12. Lai, J.; Wang, G.W.; Wang, Z.Y.; Chen, J.; Pang, X.J.; Wang, S.C.; Zhou, Z.L.; He, Z.B.; Qin, Z.Q.; Fan, X.Q. A review on pore structure characterization in tight sandstones. *Earth-Sci. Rev.* **2018**, *177*, 436–457. [CrossRef]

13. Liu, X.F.; Guo, X.D.; Hong, Z.L.; Xue, X.P.; Li, S.F. Pore Structure Characteristics and Main Control Factors of Sandstone in the Jurassic Zhiluo Formation in the Northern Ordos Basin. *Minerals* **2023**, *13*, 1102. [CrossRef]

14. Du, X.Y.; Jin, Z.J.; Zeng, L.B.; Liu, G.P.; He, W.J.; Ostadhassan, M.; Liang, X.P.; Yang, S.; Lu, G.Q. Characteristics and Controlling Factors of Natural Fractures in Deep Lacustrine Shale Oil Reservoirs of the Permian Fengcheng Formation in the Mahu Sag, Junggar Basin, China. *J. Struct. Geol.* **2023**, *175*, 104923. [CrossRef]

15. Wu, J.B.; Yang, S.L.; Gan, B.W.; Cao, Y.S.; Zhou, W.; Kou, G.; Wang, Z.Q.; Li, Q.; Dong, W.G.; Zhao, B.B. Pore Structure and Movable Fluid Characteristics of Typical Sedimentary Lithofacies in a Tight Conglomerate Reservoir, Mahu Depression, Northwest China. *ACS Omega* **2021**, *6*, 23243–23261. [CrossRef] [PubMed]

16. Ding, Y.; Zhu, R. Petrological Characteristics and Sedimentary Environment Significance of Mahu Depression of Baikouquan Conglomerate in Junggar Basin. *China's Manganese Ind.* **2017**, *35*, 9–12. [CrossRef]

17. Wang, D.Y.; Li, M.J.; Zhou, Y.; Yang, L.; Yang, Y.F.; Li, E.T.; Jin, J.; Zou, X.; Xu, B.D. Petroleum Geochemistry and Origin of Shallow-buried Saline Lacustrine Oils in the Slope Zone of the Mahu Sag, Junggar Basin, Nw China. *Pet. Sci.* **2023**, *20*, 3363–3378. [CrossRef]

18. Tan, F.Q.; Ma, C.M.; Zhang, X.Y.; Zhang, J.G.; Tan, L.; Zhao, D.D.; Li, X.K.; Jing, Y.Q. Migration Rule of Crude Oil in Microscopic Pore Throat of the Low-permeability Conglomerate Reservoir in Mahu Sag, Junggar Basin. *Energies* **2022**, *15*, 7359. [CrossRef]

19. Zhang, G.Y.; Wang, Z.Z.; Guo, X.G.; Sun, Y.N.; Sun, L.; Pan, L. Characteristics of Lacustrine Dolomitic Rock Reservoir and Accumulation of Tight Oil in the Permian Fengcheng Formation, the Western Slope of the Mahu Sag, Junggar Basin, Nw China. *J. Asian Earth Sci.* **2019**, *178*, 64–80. [CrossRef]

20. Wang, Z.Q.; Ge, H.K.; Zhou, W.; Wei, Y.; Wang, B.; Liu, S.; Zhou, H.; Du, S.H. Characterization of Pores and Microfractures in Tight Conglomerate Reservoirs. *Int. J. Hydrogen Energy* **2022**, *47*, 26901–26914. [CrossRef]

21. Cao, J.; Yao, S.P.; Jin, Z.J.; Hu, W.X.; Zhang, Y.J.; Wang, X.L.; Zhang, Y.Q.; Tang, Y. Petroleum migration and mixing in the northwestern Junggar Basin (NW China): Constraints from oil-bearing fluid inclusion analyses. *Org. Geochem.* **2006**, *37*, 827–846. [CrossRef]

22. Wang, Y.J.; Jia, D.; Pan, J.G.; Wei, D.T.; Tang, Y.; Wang, G.D.; Wei, C.R.; Ma, D.L. Multiple-phase tectonic superposition and reworking in the Junggar Basin of northwestern China—Implications for deep-seated petroleum exploration. *Aapg Bull.* **2018**, *102*, 1489–1521. [CrossRef]

23. Chen, Y.B.; Cheng, X.G.; Zhang, H.; Li, C.Y.; Ma, Y.P.; Wang, G.D. Fault characteristics and control on hydrocarbon accumulation of middle-shallow layers in the slope zone of Mahu sag, Junggar Basin, NW China. *Pet. Explor. Dev.* **2018**, *45*, 1050–1060. [CrossRef]

24. Bai, B.; Liang, J.W.; Dai, C.C.; He, W.J.; Bai, Y.; Chang, X.B.; Zheng, M.; Li, H.L.; Zong, H. Diagenesis of the Permian Fengcheng Formation in the Mahu Sag, Junggar Basin, China. *Appl. Sci.* **2023**, *13*, 13186. [CrossRef]

25. Wang, J.; Zhou, L.; Liu, J.; Li, E.T.; Xian, B.Z. Genesis of Diagenetic Zeolites and Their Impact on Reservoir Formation in the Middle Permian Lower-wuerhe Formation of the Mahu Sag, Junggar Basin, Northwest China. *Energy Explor. Exploit.* **2020**, *38*, 2541–2557. [CrossRef]

26. Hu, T.; Jiang, F.J.; Pang, X.Q.; Liu, Y.; Wu, G.Y.; Zhou, K.; Xiao, H.Y.; Jiang, Z.X.; Li, M.W.; Jiang, S.; et al. Identification and evaluation of shale oil micro-migration and its petroleum geological significance. *Pet. Explor. Dev.* **2024**, *51*, 114–126. [CrossRef]

27. Cai, G.Y.; Gu, Y.F.; Jiang, Y.Q.; Wang, Z.L. Pore Structure and Fluid Evaluation of Deep Organic-Rich Marine Shale: A Case Study from Wufeng–Longmaxi Formation of Southern Sichuan Basin. *Appl. Sci.* **2023**, *13*, 7827. [CrossRef]

28. Misch, D.; Klaver, J.; Gross, D.; Mayer-kiener, V.; Mendez-martin, F.; Schmatz, J.; Sachsenhofer, R.F. Factors Controlling Shale Microstructure and Porosity: A Case Study on Upper Visean Rudov Beds from the Ukrainian Dneiper–donets Basin. *Aapg Bull.* **2018**, *102*, 2629–2654. [CrossRef]

29. Fleury, M.; Gimmi, T.; Mazurek, M. Porewater Content, Pore Structure and Water Mobility in Clays and Shales from Nmr Methods. *Clays Clay Miner.* **2022**, *70*, 417–437. [CrossRef]

30. Guo, Y.C.; Fang, X.X.; Wang, H.F.; Wang, N. Mineralogy and Pore Structure of Marine–Continental Transitional Shale: A Case Study of the Upper Carboniferous Keluke Formation in the Eastern Qaidam Basin, China. *Front. Earth Sci.* **2022**, *9*, 825173. [CrossRef]

31. Hazra, B.; Varma, A.K.; Bandopadhyay, A.K.; Chakravarty, S.; Buragohain, J.; Samad, S.K.; Prasad, A.K. FTIR, XRF, XRD and SEM characteristics of Permian shales, India. *J. Nat. Gas Sci. Eng.* **2016**, *32*, 239–255. [CrossRef]

32. Wu, J.; Liang, C.; Hu, Z.; Yang, R.; Xie, J.; Wang, R.; Zhao, J. Sedimentation mechanisms and enrichment of organic matter in the Ordovician Wufeng Formation-Silurian Longmaxi Formation in the Sichuan Basin. *Mar. Pet. Geol.* **2019**, *101*, 556–565. [CrossRef]

33. Wu, J.; Li, H.; Goodarzi, F.; Min, X.; Cao, W.X.; Huang, L.J.; Pan, Y.Y.; Luo, Q.Y. Geochemistry and Depositional Environment of the Mesoproterozoic Xiamaling Shales, Northern North China. *J. Pet. Sci. Eng.* **2022**, *215*, 110730. [CrossRef]

34. Zhang, Q.; Wu, X.S.; Radwan, A.E.; Wang, B.H.; Wang, K.; Tian, H.Y.; Yin, S. Diagenesis of continental tight sandstone and its control on reservoir quality: A case study of the Quan 3 member of the cretaceous Quantou Formation, Fuxin uplift, Songliao Basin. *Mar. Pet. Geol.* **2022**, *145*, 105883. [CrossRef]

35. Han, Z.Y.; Wang, G.W.; Wu, H.L.; Feng, Z.; Tian, H.; Xie, Y.Y.; Wu, H. Lithofacies Characteristics of Gulong Shale and Its Influence on Reservoir Physical Properties. *Energies* **2024**, *17*, 779. [CrossRef]

36. Long, S.X.; Peng, Y.M.; Lu, J.; Zhu, T.; Sun, C.X.; Luo, J. Identification and Applications of Micro to Macroscale Shale Lithofacies. *J. Nanosci. Nanotechnol.* **2021**, *21*, 659–669. [CrossRef]

37. Li, X.; Zhou, W.; Zhou, Q.; Wu, R.B.; Yang, Z.B.; Wang, Y.T.; Peng, X.H.; Liang, T. Study on Permian Sedimentary Environment and Reservoir Characteristics in Mahu Sag, Junggar Basin, China. *Fresenius Environ. Bull.* **2021**, *30*, 8886–8898.

38. Dong, T.; Kang, L.; Zhang, Y.F.; Gao, Y. Pore Fractal Characteristics of Lacustrine Shale of Upper Cretaceous Nenjiang Formation from the Songliao Basin, Ne China. *Appl. Sci.* **2023**, *13*, 4295. [CrossRef]

39. Jia, Z.J.; Hou, D.J.; He, J.H. Sedimentary Environment and Enrichment of Organic Matter in the Shahejie Formation, Huanghekou Depression, Bohai Bay Basin, China. *Appl. Sci.* **2024**, *14*, 4547. [CrossRef]

40. Yang, Z.X.; Wang, X.Q.; Ge, H.K.; Zhu, J.X.; Wen, Y.Q. Study on Evaluation Method of Fracture Forming Ability of Shale Oil Reservoirs in Fengcheng Formation, Mahu Sag. *J. Pet. Sci. Eng.* **2022**, *215*, 110576. [CrossRef]

41. Wang, S.P.; Ma, C.F.; Sun, X.; Liu, S.L. Lacustrine Shale Diagenesis—A Case Study of the Second Member of the Funing Formation in the Subei Basin. *Processes* **2023**, *11*, 2009. [CrossRef]